

1     **An updated evaluation of the global mean Land Surface Air**  
2             **Temperature and Surface Temperature trends based on**  
3                     **CLSAT and CMST**

4             Qingxiang LI<sup>1#</sup>, Wenbin Sun<sup>1</sup>, Xiang YUN<sup>2</sup>, Boyin HUANG<sup>3</sup>, Wenjie DONG<sup>1</sup>,  
5                     Xiaolan L. WANG<sup>4</sup>, Panmao ZHAI<sup>2</sup>, Phil JONES<sup>5</sup>

6             1 School of Atmospheric Sciences and Guangdong Province Key Laboratory for Climate Change  
7             and Natural Disasters, SUN Yat-Sen University, Guangzhou, China

8             2 Chinese Academy of Meteorological Sciences, CMA, Beijing, China

9             3 National Centers of Environmental Information, NOAA, Asheville, USA

10            4 Climate Research Division, Environment and Climate Change Canada, Toronto, Canada

11            5 Climate Research Unit, University of East Anglia, Norwich, UK

12            # Key Laboratory of Tropical Atmosphere-Ocean System (Sun Yat-sen University), Ministry of Education, and Southern  
13            Laboratory of Ocean Science and Engineering (Guangdong Zhuhai), Zhuhai, China

14

15

16                             Submitted to *Climate Dynamics*

17                                     Aug 2020

18

19

20     **\*Corresponding author:**

21

22     Dr. & Prof. Qingxiang Li

23     School of Atmospheric Sciences

24     Sun Yat-Sen University

25     Tangjiawan, Zhuhai Campus of SYSU

26     Zhuhai, China, 519082

27     Tel/Fax: 86-756-3668352

28     E-Mail: liqingx5@mail.sysu.edu.cn

29

30

31

## Abstract

32 Past versions of global surface temperature (ST) datasets have been shown to  
33 have underestimated the recent warming trend over 1998-2012. This study uses a  
34 newly updated global land surface air temperature and a land and marine surface  
35 temperature dataset, referred to as China global Land Surface Air Temperature  
36 (C-LSAT) and China Merged Surface Temperature (CMST), to estimate trends in the  
37 global mean ST (combining land surface air temperature and sea surface temperature  
38 anomalies) with the data uncertainties being taken into account. Comparing with  
39 existing datasets, the statistical significance of the global mean ST warming trend  
40 during the past century (1900–2017) remains unchanged, while the recent warming  
41 trend during the “hiatus” period (1998~2012) increases obviously, which is  
42 statistically significant at 95% level when fitting uncertainty is considered as in  
43 previous studies (including IPCC AR5) and is significant at 90% level when both  
44 fitting and data uncertainties are considered. Our analysis shows that the global mean  
45 ST warming trends in this short period become closer among the newly developed  
46 global observational data (CMST), remotely sensed/Buoy network infilled datasets,

47 and reanalysis data. Based on the new datasets, the warming trends of global mean  
48 land SAT as derived from C-LSAT 2.0 for the period of 1979-2019, 1951-2019,  
49 1900-2019 and 1850-2019 were estimated to be 0.296, 0.219, 0.119 and  
50 0.081 °C/decade, respectively. The warming trends of global mean ST as derived  
51 from CMST for the periods of 1998-2019, 1979-2019, 1951-2019 and 1900-2019  
52 were estimated to be 0.195, 0.173, 0.145 and 0.091 °C/decade, respectively.

53

54 Keywords: Global Mean Surface Temperature (GMST); Global Land surface air  
55 temperature (GLSAT); Sea surface temperature (SST); Trends; Dataset

56

57

## 58 1. Introduction

59 The latest two IPCC scientific assessment reports (IPCC, 2007, 2013) pointed  
60 out that the warming of the climate system is unequivocal. The Global Mean Surface  
61 Temperature (GMST) is inferred from the land surface air temperature (LSAT) and  
62 sea surface temperature (SST) from in situ observations. Previous studies have shown  
63 that differences in the estimates of short-term trends are still relatively large, which  
64 prompted a debate within the climate community about a “hiatus” or “slowdown” in  
65 the warming over the 15 years following the 1997/1998 El Niño event (Cahill et al.,  
66 2015; Lewandowsky et al., 2015; Karl et al., 2015; Fyfe et al., 2016; Simmons et al.,  
67 2017; Rahmstorf et al., 2017; Medhaug et al., 2017; Lewandowsky et al., 2018;  
68 Risbey et al., 2018).

69 Over the past 30 years, several global LSAT datasets have been developed and  
70 have continuously been improved (Jones and Wigley, 2010; Hartmann et al., 2013;  
71 Hawkins and Jones, 2013). These include CRUTEM (Jones and Moberg, 2003; Jones  
72 et al., 2012), GHCN (Peterson and Vose, 1997; Smith and Reynolds, 2005; Smith et  
73 al., 2008; Lawrimore et al., 2011; Menne et al., 2019), GISTEMP (Hansen et al., 1999,

74 2001, 2006; Lessen et al., 2019), Berkeley Earth Surface Temperature (BEST)  
75 (Muller et al., 2013). Lugina et al (2006) and the Japan Meteorological Agency (JMA)  
76 also released their own datasets in recent years  
77 ([http://ds.data.jma.go.jp/tcc/tcc/products/gwp/temp/ann\\_wld.html](http://ds.data.jma.go.jp/tcc/tcc/products/gwp/temp/ann_wld.html)). With the  
78 continuous collection of climate data, improvements to data quality control and  
79 assurance technology and to the various spatio-temporal analysis methods, the trends  
80 of global/hemispheric mean LSATs have been updated by different research institutes  
81 (Hartmann et al., 2013). The demand for accurately estimating the magnitude of  
82 LSAT trends in monitoring climate change on global and regional scales is increasing  
83 day by day (Stott and Thorne, 2010). Recently, an international effort from China Sun  
84 Yat-Sen University (SYSU) and China Meteorological Administration (CMA), UK  
85 University of East Anglia (UEA), Environment and Climate Change Canada (ECCC),  
86 Australia Bureau of Meteorology (BOM) and USA State University of New York  
87 (SUNY) Albany published a new homogenized and integrated global LSAT dataset  
88 (C-LSAT), partly addresses this requirement (Xu et al., 2018).

89 Several SST data sets have also been developed by independent groups and are

90 available for study, with several of these updated monthly or more frequently. Some  
91 analyses use only in situ observations, prominent examples being the Extended  
92 Reconstructed SST (ERSST; Smith et al., 1996; Huang et al., 2015, 2017a), UK  
93 Hadley SST version 3 and version 4 (HadSST3/4, Kennedy et al., 2011a; 2011b;  
94 2019), and JMA's Centennial Observation-Based Estimates of SSTs (COBE-SST;  
95 Ishii et al., 2005), COBE-SST version 2 (COBE-SST2; Hirahara et al., 2014). The  
96 most recent ERSST version (ERSSTv5) and HadSST4 use newly released data  
97 archives from International Comprehensive Ocean-Atmosphere Data Set (ICOADS)  
98 3.0 (Freeman et al., 2017), which improves SST spatial and temporal variabilities  
99 and absolute SST (Huang et al., 2017a, 2018). HadSST is used in HadCRUT and  
100 Berkley Earth (BE) analysis. ERSSTv5 is used in NOAA GlobalTempv5 (Zhang et al.,  
101 2019) and GISTEMP (Hansen et al., 1999, 2001, 2006; Lessen et al., 2019) analyses.

102 IPCC's AR5 (IPCC, 2013) pointed out that, when updates have been made to all  
103 three GMST datasets (Hansen et al., 2010; Morice et al., 2012; Vose et al., 2012) used  
104 in AR4 (IPCC, 2007), GMSTs are in a somewhat better agreement with each other  
105 over recent years. For example, HadCRUT4 now has better sampling over the

106 Northern Hemisphere high latitude land areas (Jones et al.,2012; Morice et al., 2012)  
107 in contrast toHadCRUT3 showed an underestimation of recent warming (Simmons et  
108 al., 2010). Recently, scientists have concluded that differences in how datasets handle  
109 data sparse areas such as the polar regions can result in a sampling "bias" of surface  
110 air temperature (SAT), especially in the so-called "hiatus" period during 1998-2012.  
111 (Cowtan and Way, 2014 and 2018; Karl et al., 2015; Huang et al., 2017a; Simmons et  
112 al., 2017). Cowtan and Way (2014) developed a hybrid version of global surface  
113 temperature: Satellite data were used to reconstruct an SAT series in the regions that  
114 are not covered by HadCRUT4 data (about 16% of global area by their evaluation,  
115 including polar regions and parts of Africa and South America), which increases the  
116 temperature trend from 0.046°C/decade to 0.119°C/decade for the period of  
117 1997-2012. Huang et al. (2017b) interpolated data from the International Arctic Buoy  
118 Observatory (IABO) data and found that the trend of warming was 0.112°C/decade  
119 over the period 1998-2012, which is higher than the trend in the  
120 NOAAGlobalTempv4 (formerly Merged Land and Ocean Surface Temperature  
121 dataset (MLOST)) data over the same period (about 0.050 °C/decade). Also Zhang et

122 al. (2019) showed that the updated surface temperature data tends to give a more  
123 consistent view of climate trends (from 0.070 °C/decade in v4 to 0.073 °C/decade in  
124 v5 during 1880-2018). Simmons et al. (2017) showed that the infilled observational  
125 datasets agreed better with both ERA-Interim and JRA-55 reanalysis and provided  
126 similar global mean surface warming trends since 1979, but their warming trends over  
127 1998-2012 (0.140 and 0.090 °C/decade) were larger than any of the in situ  
128 observational datasets used in IPCC 5<sup>th</sup> Assessment Report (AR5) (Hartmann et al.,  
129 2013).

130 In this paper, we used a new merged global ST dataset: China global Merged  
131 Surface Temperature (CMST; Yun et al., 2019; Li et al., 2020a) based on the most  
132 recently published C-LSAT (Xu et al., 2018) and ERSST v5 (Huang et al., 2017a)  
133 datasets. A systematic comparison is conducted on the global LSAT and ST trends  
134 during the “hiatus” or “slowdown” period (1998-2012) among the existing datasets.  
135 Based on these, we present a new evaluation of the global ST trends.

136 This paper is arranged as follows: the datasets and the methodology are briefly  
137 introduced in section 2; the update of the C-LSAT and the trends evaluation for



138 different time scales are introduced in section 3; the analysis results are given in  
139 section 4; some reasons for the differences and uncertainty assessment of global ST  
140 changes are discussed in section 5, and the conclusions are presented in section 6.

## 141 **2. Datasets and their processing methods**

### 142 2.1 LSAT and SST datasets

143 A total of 14 data sources have been collected and integrated into the C-LSAT  
144 dataset including three global (CRUTEM4, GHCN, and Berkeley SAT), three  
145 regional sources and eight national sources (including homogenized datasets from  
146 Australia, Canada, China, and the United States). Inhomogeneities in the data series  
147 are detected and adjusted for using a penalized maximal t-test (50% of all stations),  
148 then the station series are converted into  $5^\circ \times 5^\circ$  latitude by longitude grids data (for  
149 complete details see Xu et al., 2018). The C-LSAT version used in this paper includes  
150 the update described in Yun et al. (2019) and Li et al. (2020a), and will be detailed  
151 described in section 3. The newly updated China global Land Surface Air  
152 Temperature dataset (C-LSAT version 2.0) is available at  
153 <https://doi.pangaea.de/10.1594/PANGAEA.919574>.

154 In this paper, several other LSAT datasets including Climatic Research Unit  
155 (CRU) CRUTEM4, NOAA Global Historical Climate Network dataset (GHCN) v3,  
156 Berkeley SAT and NASA GISTEMPv3 (all were downloaded in July 2018) are also  
157 used to calculate/compare global LSAT trends. For consistency, the time periods for  
158 all the datasets have been set to Jan 1900 to Dec 2017 (in and after section 4). For  
159 CRUTEM4, we use the latest version CRUTEM4.6. GISTEMP has two versions with  
160 different degrees of spatial smoothing: 250km and 1200km. GISTEMP (1200km)  
161 starts in 1880 and GISTEMP (250km) starts in 1902. GHCNv3 has the same  
162 resolution as C-LSAT and CRUTEM4, and Berkeley SAT is at  $1^{\circ} \times 1^{\circ}$  latitude by  
163 longitude resolution, which has been interpolated using Kriging methods.

164 Of the SST datasets mentioned in section 1, two (HadSST and ERSST) have  
165 been used to merge with LSAT to develop global ST datasets to assess global surface  
166 warming trends. ERSSTv5 (Huang et al., 2017a) uses new data sets from ICOADS  
167 Release 3.0 SST (Freeman et al., 2017), measurements from Argo floats down to 5  
168 meters depth, and Hadley Centre Ice-SST version 2 (HadISST2) (Titchner and Rayner,  
169 2013) ice concentrations. ERSSTv5 has improved SST spatial and temporal

170 variability and absolute SST. HadSST3 is an ensemble dataset, the median of the 100  
171 ensembles of HadSST3 is adopted to calculate the SST trends. For comparison, both  
172 SST datasets have been used to merge with C-LSAT, respectively, in this paper.

## 173 2.2 Global ST datasets

174 After systematic comparisons, CMST was developed based on the C-LSAT and  
175 ERSSTv5 (Yun et al., 2019; Li et al., 2020a) and used to calculate long-term trends of  
176 GMST, similar to what was undertaken in Vose et al. (2012). The C-LSAT and  
177 ERSSTv5 are merged as follows: The monthly SSTs on  $2^{\circ}\times 2^{\circ}$  grids and LSATs on  
178  $5^{\circ}\times 5^{\circ}$  grids are both first interpolated to  $1^{\circ}\times 1^{\circ}$  grid, which is distributed in four grids  
179 of  $1^{\circ}\times 1^{\circ}$  for SSTs and in 25 grids of  $1^{\circ}\times 1^{\circ}$  for LSATs, and then box-averaged to  $5^{\circ}\times 5^{\circ}$   
180 deg grids according to the ratio between ocean and land areas for each individual grid  
181 box (Yun et al., 2019). The newly CMST dataset is available at  
182 <https://doi.pangaea.de/10.1594/PANGAEA.919662>.

183 The GMST series are calculated as follows: LSAT and SST anomalies are  
184 calculated relative to the reference period 1961-1990, and only those stations/grids  
185 with at least 15 years of values during 1961-1990 are calculated. The gridding of the

186 land surface air temperature anomalies is undertaken by averaging all values within 5 °  
187 × 5 ° grids (Jones and Moberg, 2003; Xu et al., 2018). Regional (North Hemisphere,  
188 South Hemisphere, and Tropics) series are calculated in the same way.

189 Four other global observation-based ST datasets including HadCRUT4,  
190 NOAAGlobalTempv4, Berkeley Earth (BE), and GISS v3 (downloaded in July 2018)  
191 are also analyzed in this paper (each with time periods set to Jan 1900 to Dec 2017).

192 Of these, BE provided two versions of merged global ST datasets, which differ in how  
193 the sea ice is treated. In the first version (BE1), temperature anomalies in the presence  
194 of sea ice are extrapolated from land-surface air temperature anomalies. In the second  
195 version (BE2), the anomalies are extrapolated from sea-surface water temperature  
196 anomalies (usually collected from open water areas near the periphery of the sea ice).

197 It should be noted that all the global ST datasets have been updated since the  
198 publication of IPCC AR5, so the trends may be different from those published there  
199 even if the version numbers have not been changed. For example, HadCRUT4 used  
200 an earlier version of CRUTEM4 in AR5, but has been updated to CRUTEM4.6 at  
201 present; MLOST has been replaced by NOAAGlobalTempv4 since 2015, and GISS

202 has been updated several times on its use of SST datasets (currently, it uses ERSSTv5)  
203 and its uncertainty model (Lenssen et al., 2019).

204 Two other global ST analyses for shorter periods are also used in this paper. They  
205 are the comprehensively analyzed ECMWF ERA5 (Hersbach et al., 2020) and  
206 HadCRUT4 hybrid (Cowtan and Way, 2014). ERA5 provides a 2m temperature  
207 product from optimal-interpolation analyses of screen-level observations, using  
208 background fields provided by their main 4D-Var data assimilation schemes (with  
209 more observational data input along with CMIP5 greenhouse gases, volcanic  
210 eruptions, SST and sea-ice cover as the model input). In this study, we also used the  
211 ERA5 analysis fields over the land and the background fields over the oceans  
212 (<https://climate.copernicus.eu/climate-bulletin-about-data-and-analysis>) (Hersbach et  
213 al., 2020). The HadCRUT4 hybrid is the HadCRUT4 infilled using data from the  
214 University of Alabama in Huntsville (UAH) satellite data. Here, we use the median of  
215 the ensembles from HadCRUT4 as in Cowtan and Way (2014). Both of these two  
216 datasets cover the period from January 1979 to December 2017.

217 2.3 Estimation of trend and its uncertainty

218 The fitting uncertainty arises because there are many and various combinations  
219 of trend, natural variability, and noise that could have combined into the observed  
220 series. Usually, the trend and its uncertainty at the 95% confidence interval are  
221 expressed as  $\beta \pm \delta$  where  $\beta$  corresponds to the range of trends that have 5% or less  
222 chance of occurring. This is based on the assumption that the annual temperature  
223 samples are approximately Gaussian distributed. But sample size also matters: The  
224 smaller the sample size, the more challenging it is to obtain good accuracy for trend  
225 estimates. Estimates of trend over a shorter period (like the period 1998-2012) are  
226 thus more challenging. Similar to IPCC (2013), the long-term trends of global GMST  
227 and GMSAT and their significance at the 95% level ( $\sim 1.96$  sigma) are calculated by  
228 using the method of Restricted Maximum Likelihood Regression (REML; Diggle et  
229 al., 1994). The REML method is the basic method used to calculate climate change  
230 trend since IPCC TAR. Since the autocorrelation of temperature series has been  
231 considered, it is more insensitive to extreme values than ordinary least squares.  
232 Therefore, it is more suitable to be used as a calculation method of climate change  
233 trend, especially for climate elements with autocorrelation such as temperature. So the

234 trends and their uncertainties are mostly estimated based on REML (Tables 1-4).

235       However, recent studies (Cahill et al., 2015; Rahmstorf et al., 2017) stated that  
236 almost every treatment of the significance of “hiatus” trends, including the IPCC  
237 reports, was based on an uncertainty method without consideration of the data  
238 uncertainties (the autocorrelation of the residual of linear fitting has not been  
239 considered) and has overestimated the significance of the change in trend. Although  
240 the existing global LSAT and SST datasets have generally been thought reliable, the  
241 uncertainties in global and regional ST during the past 100 years still attracts attention  
242 in recent studies (Brohan et al., 2006; Li et al., 2010; Kennedy et al., 2011a, b; Morice  
243 et al., 2012; Hartmann et al., 2013; Kennedy, 2014; Karl et al., 2015; Huang et al.,  
244 2015; 2017a; Li et al., 2017). According to Brohan et al. (2006) and Kennedy et al.  
245 (2011a; 2011b), uncertainties in the LSAT and SST are divided into 3 types: (1)  
246 station error (measurement error), (2) sampling error, and (3) bias error. Of these, the  
247 bias error is the most important at long-term and large scales and is the most clearly  
248 expressed in long-term trends in the global average SST. Sampling errors are the most  
249 important at regional scales especially for the regions with relatively sparse

250 observations (Li et al., 2020b; Li and Yang, 2019).

251 To compare with the significance of the GMST trends, in this study we estimated  
252 the data uncertainty using the spread of linear trends estimated from the time series  
253 that is perturbed by its standard deviation (STD) (Figure 1), following the similar  
254 approach of Karl et al. (2015) : (1) a time series is detrended; (2) the STD of the  
255 detrended time series is calculated; (3) a random temperature perturbation is selected  
256 based on a Gaussian distribution with zero mean and STD in (2); (4) a 1000-member  
257 ensemble time series is generated; (5) linear trend and its fitting uncertainty is  
258 calculated for all 1000 members; (6) the STD of the trend is defined as the data  
259 uncertainty, and the ensemble averaged fitting uncertainty is defined as the final  
260 fitting uncertainty; (7) the total uncertainty is defined as the root square mean of the  
261 data uncertainty and final fitting uncertainty. This provides an ensemble approach for  
262 evaluating the total uncertainties and the significance of the GMST trend. The results  
263 are given in Table 5.

### 264 **3. Update of C-LSAT and its uncertainties evaluation**

#### 265 **3.1 Interannual variation of LSAT anomaly and its uncertainty**



266 Much progress has been made in the uncertainties estimation of the observational  
267 datasets (Brohan et al., 2006; Folland et al., 2001; Li et al., 2010; 2020a; Wang et al.,  
268 2014; Kent et al., 2017; Menne et al., 2018; Huang et al., 2019; Lesson et al., 2019) .  
269 The model produced by the Brohan et al. (2006) and Li et al. (2010) is used in this  
270 article. In this model uncertainties in the land data are divided into three types: (1) the  
271 uncertainties of individual station anomalies (station error); (2) the uncertainties in a  
272 grid box mean caused by estimating the mean from a small number of point values  
273 (sampling error); and (3) the uncertainties in large-scale temperatures caused by  
274 systematic changes in measurement methods (bias error). The total uncertainties value  
275 for any grid box can be obtained by adding the square root of the three errors.

276 Figure 2 shows the best estimate of GLSAT anomaly and its 95% uncertainty  
277 range arising from station error, sampling error, bias error, and spatial coverage errors.  
278 It can be seen in the figure that the sampling error and station error have become  
279 smaller with time, and have remained stable after the 1950s. The greater uncertainty  
280 of the series in the first 50 years comes from insufficient data coverage; and the  
281 temperature series shows significantly larger inter-annual variability in the 50 years

282 before the 20th century due to the scarcity of station distribution. Inter-annual  
283 variability becomes much smaller after 1900, which is somewhat similar to the LSAT  
284 variability in China (Li et al., 2010; Li et al., 2017). The only difference is that the  
285 uncertainty of GLSAT is smaller than that at the regional scale (Li et al., 2020b).

286 The GLSAT fluctuated from 1850s to the late 1970s. The series reached an  
287 extreme value (anomaly  $0.18^{\circ}\text{C}$ ) in 1878, sharply decreased during the middle and  
288 late 1880s, rose again till the late 1930s, and reached another extreme value  
289 (anomaly  $0.26^{\circ}\text{C}$ ) in 1938. The series then experienced a relatively cooling period to  
290 the mid-1960s, and then entered a continuously rapid warming period when it reached  
291 a new extreme value (anomaly  $1.40^{\circ}\text{C}$ ) in 2016. It slightly declined in recent years,  
292 but remained high with the fourth (2017, anomaly  $1.18^{\circ}\text{C}$ ), sixth place (2018,  
293 anomaly  $0.96^{\circ}\text{C}$ ) and third place (2019, anomaly  $1.24^{\circ}\text{C}$ ) since 1850s. If we calculate  
294 the difference between the GLSAT anomalies in the last 10 years and those for the  
295 pre-industrial period (represented by the 1850-1900 averages), the number is  $1.52^{\circ}\text{C}$   
296 (about  $1.40^{\circ}\text{C}$  for the last 20 years). That is, the GLSAT has now risen close to  $1.50^{\circ}\text{C}$   
297 from the pre-industrial period.

298 Judging from the 95% uncertainty range the GLSAT series (the inset of Figure  
299 2a), the annual uncertainties were greater than 0.2°C during the period of 1850 - 1880,  
300 after which they dropped to 0.15°C and below during the period of 1881-1900; and  
301 after 1901 they dropped to 0.1°C and below reaching their lowest value of about  
302 0.07°C after 1951. This result is very close to GISSTEMP, GHCN4, Berkeley SAT,  
303 and CRUTEM4 (Lesson et al., 2019), which also show that the current accuracy is  
304 broadly similar among the existing GLSAT datasets in describing the GLSAT change  
305 (Li et al., 2020a).

### 306 **3.2 Long-term trends of GLSAT and their uncertainties**

307 The long-term trend of GLSAT anomaly from 1850 to 2019 and the 95%  
308 uncertainties range were calculated for several periods (Table 1). Regardless of  
309 whether only the fitting uncertainty is considered, or the fitting and data uncertainty  
310 are fully considered, the trends of LSAT changes in 1850-2019, 1901-2019,  
311 1951-2019, 1979-2019 and 1998-2019 all significantly positive at 5% level, with the  
312 linear trends of  $0.081 \pm 0.014$ ,  $0.119 \pm 0.023$ ,  $0.219 \pm 0.042$ ,  $0.296 \pm 0.077$ , and  $0.234$   
313  $\pm 0.198^\circ\text{C}$  per decade, respectively. Among these, since 1979, the surface air

314 temperature has risen close to 0.3°C every 10 years, which is the period of fastest  
315 warming since the record began in the middle of the 19th century.

#### 316 **4. Comparison and evaluation on the global LSAT and ST trends**

##### 317 4.1 Comparisons on global LSAT and ST trends since 1998

###### 318 4.1.1 Global LSAT changes

319 Xu et al. (2018) showed that C-LSAT obtained similar SAT trends to those in  
320 CRUTEM4 and GHCNv3 in continental areas for the period 1900-2014 (with faster  
321 warming rates in Asia and slower in Africa and Antarctica (1951-2014)) (their Tables  
322 5 and 6). Figure 2 shows the distribution of the linear trends for SAT in all the grid  
323 boxes for the six datasets: C-LSAT, CRUTEM4.6, GHCNv3, GISTEMPv3 (200km  
324 and 1200km) and Berkeley SAT. GISTEMP and Berkeley SATs use similar station  
325 distributions to GHCNv3. It is worth mentioning that there are strong spatial  
326 variations in some neighboring grid boxes for the shorter-term periods (Figure 3a),  
327 which is also occasionally found in other datasets (Figures 3 b-d) due to the different  
328 lengths of the data series (Xu et al., 2018). Obviously, C-LSAT has the greatest  
329 coverage in comparison with other datasets especially in the higher latitude regions

330 (Arctic and Antarctic) and the Tropics (30°S-30°N) (Figure 3; Xu et al., 2018 and Yun  
331 et al., 2019) except for GISTEMP (1200km smoothing) and Berkeley SAT due to  
332 spatial smoothing and infilling. C-LSAT includes more than 1,000 station data series  
333 in the Arctic (60°N-90°N), which is much more than those used in CRUTEM4 and  
334 GHCNv3/GISTEMPv3 (but no more data in the Antarctic) during 1998-2012 (Figures  
335 2a-f). Figure 4 shows the annual mean LSAT anomaly series for C-LSAT, CRUTEM4,  
336 and GHCNv3 in the Arctic (land area in 60°-90°N) and at global scales in all 5  
337 datasets during 1998-2012 (1998-2017). In the Arctic, the linear trends of LSAT are  
338 calculated for different datasets as follows: 0.747, 0.798, and 0.559°C/decade,  
339 respectively (Figure 4a). The former two are much larger than the latter one, which  
340 agrees well with Cowtan and Way (2014) and Huang et al. (2017b). We also notice  
341 that the linear trend of LSAT has been changed to 0.080 °C/decade for GHCNv4,  
342 which further shows the trend in this region was underestimated for GHCNv3  
343 (0.052 °C/decade, Table 2).

344 At the global scale, the linear trends for LSAT are calculated for C-LSAT1.3,  
345 CRUTEM4.6, GHCNv3, GISTEMPv3, and BEST, respectively (Table 2). The global

346 LSAT trends in GHCNv3 and Berkeley SAT are the smallest and the largest,  
347 respectively, which is related to the higher anomalies during 1998 to 2002 for  
348 GHCNv3 and for 2007 to 2012 for Berkeley SAT analysis. Only the trend in C-LSAT  
349 is significant at the 5% level. GISTEMPv3 shows lower anomalies during the whole  
350 15-year period (Figure 4b).

351 Further, the trends of the 6 global mean LSATs for the different periods of  
352 1998-2017, 1979-2017, 1951-2017, and 1900-2017 have been calculated and shown  
353 in Table 2. The trends for 1998-2017 are all significant at the 5% level. The LSAT  
354 trend from C-LSAT is higher than those derived from CRUTEM4.6, GHCNv3, and  
355 GISTEMPv3, but similar to that from Berkeley since 1998. The differences in the  
356 warming trends among all the datasets become smaller with the extension of the time  
357 scales.

#### 358 4.1.2 Global ST changes

359 Of all the global ST datasets used in this paper, CMST, GISS and  
360 NOAAGlobalTemp use ERSST (CMST and GISSv3 use ERSSTv5, and  
361 NOAAGlobalTempv3 uses ERSSTv4, but the newly released NOAAGlobalTempv4

362 uses ERSSTv5 at present), HadCRUT4 and BE use 100 ensembles of HadSST3 (in  
363 this paper, we use the median of the 100 ensembles). Figure 5 shows the distribution  
364 of the linear trends of GMSTs in the period of 1998-2012 averaged over all available  
365 grid boxes in the six observational datasets and the other two datasets (HadCRUT  
366 Hybrid and ERA5). The main characteristics of the GMST trends are very similar to  
367 each other: Cooling trends are mostly found in East Asia (West Pacific Ocean),  
368 western North America including the northeastern North Pacific and the South Pacific.  
369 Warming trends are more significant in the high latitudes of the Northern Hemisphere.  
370 It should be noted that ST changes during the short-term period (1998- ) have more  
371 differences than those during the longer periods (1900-, 1951- and 1979- ). The latter  
372 show almost consistent warming trends at global scales (IPCC, 2007; 2013, also  
373 shown in Figure 9 of Xu et al. (2018).

374 Figure 6 shows the 6 observational global annual mean ST anomalies series,  
375 ERA5 ST series and HadCRUT Hybrid (with UAH) ST series over 1998-2012 and  
376 1998-2017 (all are relative to 1981-2010 averages). The linear trends of global ST are  
377 calculated for each dataset. They are 0.091, 0.055, 0.084, 0.071, 0.110, 0.079, 0.140,

378 and  $0.120^{\circ}\text{C}/\text{decade}$ , respectively, in CMST, HadCRUT4, NOAAGlobalTempv3,  
379 GISSv3 (1200km), BE1, BE2, ERA5, and HadCRUT Hybrid (Table 3). Of these,  
380 HadCRUT4, GISSv3, BE2, and NOAAGlobalTemp v3 (all the existing observational  
381 datasets) have similar warming trends, but lower than those during 1900-2017 and  
382 still insignificant at the 5% level. In contrast, ERA5, HadCRUT Hybrid and BE1 have  
383 much larger warming trends than others. BE1 has larger trends than BE2 because its  
384 temperature anomalies over the sea-ice area are extrapolated from land-surface air  
385 temperature anomalies instead of the nearby sea-surface water temperature anomalies  
386 in BE2. Simmons et al. (2017) showed that the recent reanalysis (ERA-Interim:  $0.140^{\circ}\text{C}$   
387  $/\text{decade}$ , and JMA-55:  $0.090^{\circ}\text{C}/\text{decade}$ ) exploited the richness of the observing system  
388 that has been in place over recent decades and extended the data coverage spatially. In  
389 this paper, our calculation indicates that the warming trends in the recently released  
390 ERA5 (Hersbach et al., 2020) were  $0.140\pm 0.112^{\circ}\text{C}/\text{decade}$  (the same as with  
391 Simmons et al. (2017) using ERA-Interim) over the periods 1998-2012. This is  
392 slightly larger than that in CMST analysis ( $0.091\pm 0.088^{\circ}\text{C}/\text{decade}$ ). Therefore, it is  
393 clear that the global "warming hiatus" trend is only a statistical artifact over this



394 period of time, as Lewandowsky et al. (2015) and Cowtan et al. (2018) pointed out.  
395 Although Medhaug et al. (2017) and other studies pointed out that there was  
396 subduction of heat into the oceans during the period 1998-2012. From the current  
397 study, this heat subduction does not lead to the “slowdown” of global warming rate.

398 Further, the CMST analyses show that the global ST warming rate for the period  
399 1998-2017 is 0.190°C/decade, which is a little larger than that over 1979-2017, much  
400 larger than that over 1951-2017 (0.133°C/decade), and more than double the rate over  
401 1900-2017 (0.086°C/decade) (Table 3). The most recent two years still continue to be  
402 warm years (2018 is the 5<sup>th</sup> warmest years, and 2019 is the 3<sup>rd</sup> warmest year), so the  
403 global ST warming rate for the period since 1998 (i.e. 1998 to 2019) would scarcely  
404 alter this evaluation (Li et al., 2020a).

## 405 4.2 Evaluation on Global and Hemispheric ST changes from CMST since 20<sup>th</sup> 406 Century

### 407 4.2.1 Global Mean ST changes

408 According to IPCC AR5, GMST has increased since the late 19th century. Each  
409 of the past four decades has been significantly warmer than all the previous decades

410 in the instrumental record, and the first and second decades of the 21<sup>st</sup> century have  
411 been the warmest two. For LSAT, Xu et al. (2018) discussed that the long-term trends  
412 for 1900-2014 evaluated from C-LSAT, CRUTEM4 and GHCNv3 are very close to  
413 each other. For Global ST change since 1880, IPCC AR5 listed 3 existing global  
414 observational datasets (HadCRUT4, NOAAGlobalTempv3 and GISSv3) and gave  
415 linear trends of  $0.062 \pm 0.012$ ,  $0.064 \pm 0.015$  and  $0.065 \pm 0.015^{\circ}\text{C}/\text{decade}$ ,  
416 respectively, for global mean ST changes over the period 1880-2012. Although the  
417 1998-2017 warming trend is significantly higher in C-LSAT than all the other existing  
418 observational datasets except for Bekerley SAT, which uses a different gridding  
419 method, the global LSAT warming trends from C-LSAT over 1900-2017 are similar to  
420 CRUTEM4.6, GHCNv3 (also see the Figures 7, 8 in Xu et al. (2018)), GISTEMPv3,  
421 and Berkeley SAT analysis (Table 2). The global ST warming trends for 1900-2017  
422 are also similar to each other for CMST, HadCRUT4, NOAAGlobalTemp, GISSv3,  
423 BE1 and BE2 (Table 3).

424 Further, we compared the GMST series derived from CMST with those derived  
425 from five other datasets during 1900-2017 and found that all the datasets agree well

426 with each other on the surface temperature changes at the global scale in the past  
427 century, and the differences mainly exist at smaller spatial or temporal scales (Figure  
428 7). Recently, we have confirmed that the consistency of the current GLSAT and  
429 GMST warming trends after 1880 is further strengthened (Li et al., 2020a).

430 Figure 8 shows the global, hemispheric and tropical (30°S to 30°N) mean ST  
431 series based on CMST over the period of 1900-2019. Although with some spatial and  
432 temporal variability of local ST, CMST showed similar decadal and long-term  
433 changes to previous studies: the global mean ST experiences rapid warming during  
434 two periods: from 1910s to mid-1940s and from mid-1970s to present. The linear  
435 trends for global and regional ST change for different time periods are given in Table  
436 4 and Table5. From Table 5, the estimated warming trends for global mean ST over  
437 1900-2019 and 1951-2019 are 0.091°C/decade and 0.145°C/decade, respectively.

#### 438 4.2.2 Hemispheric and Tropical Belt ST changes

439 Figures 8b-d show the Hemispheric and Tropical Belt ST changes during  
440 1900-2019 based on CMST, with linear trends and their 95% uncertainties listed in  
441 Table 4. We noticed that for the NH and Tropics regions, the linear trends are

442 continually increasing for the periods of 1900-2019, 1951-2019, 1979-2019, and  
443 1998-2019, which shows the totally opposite results to what might be expected from  
444 the term “warming hiatus” over 1998-2012. Exceptions happen in the SH. The linear  
445 trends and their 95% confidence intervals are  $0.077\pm 0.006$ ,  $0.113\pm 0.011$ ,  $0.079\pm 0.022$ ,  
446 and  $0.125\pm 0.055^{\circ}\text{C}/\text{decade}$  for the period 1900-2019, 1951-2019, 1979-2019, and  
447 1998-2019, respectively. These exceptions could be related to the recent cooling  
448 trends in the South Pacific region with lower warming rates over the Southern  
449 Hemisphere Oceans. It should be noted that the warming trend is greater (but with  
450 larger uncertainty) in the tropics than at global scales during the recent 20 years,  
451 which is different from that for longer term periods. The reason for the different  
452 warming trends between the tropics and global surface could be related to the  
453 relatively strong El Niño-Southern Oscillation events in recent years (Trenberth et al.,  
454 2002; Zhai et al., 2015). Table 3 also shows that the differences between the warming  
455 rates in the NH and SH were getting larger during the last century. That is, the  
456 warming in NH and the Tropics is faster than that in the SH, which may change the  
457 balance of surface atmospheric energy (Peterson et al., 2011). This also shows that

458 HadCRUT Hybrid possibly overestimating the warming trends since 1998 from the  
459 comparisons with CMST and other observational datasets (Figure 5 and their Figure 2  
460 in Cowtan and Way (2014)), especially in the Southern Hemisphere.

## 461 **5. Discussions**

### 462 5.1 Differences due to data processing methods

463 All the datasets discussed above can be divided into two types: the first type is  
464 observational datasets without interpolation (or interpolated with small scanning  
465 radius), which includes C-LSAT (CMST), CRUTEM (HadCRUT4), GHCNv3  
466 (NOAAGlobalTempv3), and GISTEMPv3-250km (GISS-250km). The other type  
467 includes all the interpolated/infilled datasets (Berkeley Earth (BE1, BE2), and  
468 GISTEMP-1200km (GISSv3-1200km)), infilled datasets (e.g., HadCRUT Hybrid),  
469 and reanalysis datasets (e.g., ERA5). It needs to be noted that GHCNv3  
470 (NOAAGlobalTempv3) and GISTEMP-250km (GISSv3-250km) indeed contain a  
471 certain degree of interpolation, but the scanning radius of interpolation is small, which  
472 is insufficient to fill the grids of all missing data over large blank areas.

473 Cowtan and Way (2014) pointed out that the incomplete global coverage is a

474 potential source of bias in global temperature reconstructions if the temperatures in  
475 the unsampled regions are not uniformly distributed over the planet's surface. The  
476 different interpolation/infilling (Kriging, UAH hybrid, IABO, Reanalysis, etc.) always  
477 leads to different results (see their Table 3). In this paper, although there are no direct  
478 relationships between the warming trends and interpolation methods, the trends are  
479 spatially relatively larger in GISSv3-1200km than those in GISSv3-250km (Figures  
480 2d and 2e), but the trends are similar in GISTEMPv3-250km and  
481 GISTEMPv3-1200km.

482 A large difference is also seen between BE1 and BE2 (Table 3). This shows that  
483 the infilling of the temperature anomalies over the sea-ice region with land-surface air  
484 temperature anomalies increases the warming trends during recent decades  
485 (1979-2017, 1998-2012 and 1998-2017). But it is interesting that the infilling  
486 decreases the trends during the longer periods (1900-2017; 1951-2017). This  
487 difference may be due to that some of the SAT data used in the infilling have been  
488 observed only during recent decades; these short ice SAT series increase the recent  
489 warming trends with better spatial sampling but were excluded when calculating

490 long-term trends. This infilling possibly brings some inhomogeneities into the  
491 global/regional mean ST changes (and using UAH satellite data hybrid procedure  
492 would have a similar issue) as Xu et al. (2018) discussed. Therefore, the  
493 reconstruction of the long-term ST series in high latitudes is still open for discussion  
494 (Karl et al., 2015; Huang et al., 2017b).

495 Our study indicates that the difference of C-LSAT from CRUTEM, GHCNv3,  
496 and GISTEMPv3-250km results from the fact that the number of used stations in Asia,  
497 Arctic, Africa, and South America is much higher in C-LSAT than GHCNv3 but only  
498 slightly higher than CRUTEM4 for the entire analysis period. But the station densities  
499 in the latter 3 regions are still relatively low (Figure 6 in Xu et al. (2018)). The  
500 differences among Global ST datasets are more complicated, but CMST obtains  
501 slightly larger trends than those from existing observational datasets, similar to that  
502 from ERA5, and closer to other reconstruction results with satellites.

## 503 5.2 The impact of SST analysis to the global mean ST trends

504 Measurements of SST have been made for more than 200 years for a wide variety  
505 of purposes. More complicated uncertainty quantification methods have been

506 proposed for historic SST datasets than those with LSAT datasets (Kennedy, 2014,  
507 Kent et al., 2017; Huang et al., 2016, 2019). Previous studies pointed out that  
508 different SST analyses may be the main contributor of the inconsistencies of global  
509 STs (Simmons et al., 2017). Here we find similar features by analyzing the results of  
510 the global merged ST changes using ERSST5 and the median of the ensemble of  
511 HadSST3 (Figure 9). The result shows that the CMST (Merge1, C-LSAT+ERSSTv5)  
512 is colder than Merge2 (C-LSAT + median of HadSST3) during 1920s -1970s, and  
513 from 2000s to present, but the long-term trends for different merging methods (for the  
514 period of 1900-2017) remain similar. These results are very similar to the differences  
515 between the HadSST3 and ERSSTv4 described in Figure 9a of Huang et al. (2016).  
516 There are some differences, however, in the trends over the longer time periods since  
517 1900, which is related to the SSTs being higher in HadSST3 than ERSSTv5 due to  
518 higher ship SST bias corrections in the 1880s–1940s and 1950s–1960s as indicated in  
519 Huang et al. (2016).

520 The linear trends and their 95% uncertainty ranges for global ST series based on  
521 the two different merged datasets are listed in Table 5. It is interesting that the



522 warming trends in CMST are all larger than those in Merge2 in different periods  
523 except for the period of 1979-2017. This is obvious because the ST anomalies in  
524 every starting year (1900, 1951 and 1998) are lower than those in the Merge2 series.  
525 That is, if we choose other start years (for example, 1979, 1981 etc.), the results could  
526 alter the opposite way. Although there are some differences in the global mean ST  
527 trends during the period of 1998-2012 between the two merges, the significances of  
528 the trends are quite similar. In addition, we noticed that the differences between the  
529 merging methods are not more than the 95% of the linear trends fitting uncertainty  
530 range.

### 531 5.3 Significance when considering both the data and fitting uncertainties

532 Note that the trend uncertainties given in the Tables 1-4 are only the fitting  
533 uncertainties. An ensemble approach has been adopted to better describe complex  
534 temporal and spatial interdependencies of measurement and bias uncertainties and to  
535 allow these correlated uncertainties to be taken into account when the time series is  
536 perturbed by data uncertainty in HadCRUT4 (Morice et al., 2012). Correlated errors  
537 in the station series are quantified by running the homogenization algorithm as an

538 ensemble in GHCNv4 (Menne et al., 2018). The uncertainties from both C-LSAT and  
539 ERSSTv5 are evaluated, respectively, and then these two are combined into the total  
540 uncertainties of CMST (Li et al., 2020a).

541 After the data uncertainties are propagated into the uncertainty of trend  
542 calculation, the significance of the GMST trends for different scales mostly remains  
543 the same except for the trend for the period of 1998-2012, which has changed from  
544  $0.091 \pm 0.088^\circ\text{C}/\text{decade}$  (significant) when only trend fitting uncertainty is included to  
545  $0.091 \pm 0.094^\circ\text{C}/\text{decade}$  (insignificant at the 95% level but significant at the 90% level)  
546 when the fitting and data uncertainties are also included (Table 5). This shows that the  
547 traditional evaluation on the uncertainties indeed overestimated the significance of  
548 trends of 1998-2012, in agreement with the previous studies (Cahill et al., 2015;  
549 Rahmstorf et al., 2017). This trend is slightly larger than those derived from existing  
550 observational datasets in HadCRUT4, NOAA GlobalTemp, GISSv3 (1200), and BE2  
551 (Berkeley dataset with SST in Polar Region) respectively. It is closer to that from  
552 ERA5, Karl et al. (2015), and the other reconstruction data sets with satellite and  
553 other kinds of observations (Cowtan and Way, 2014; Huang et al., 2017a).

## 554 6. Conclusion

555 The recently released C-LSAT dataset, with more stations at higher latitudes and  
556 improved data quality at sub-continental scales, shows broad consistency with the  
557 recent analyses of recent global LSAT changes. The trends of global mean land SAT  
558 as derived from C-LSAT2.0 for the period of 1979-2019, 1951-2019, 1900-2019 and  
559 1850-2019 were estimated to be 0.296, 0.219, 0.119 and 0.081 °C/decade,  
560 respectively.

561 When this data was merged with ERSSTv5, we have produced the new merged  
562 global ST dataset, CMST (Yun et al., 2019; Li et al., 2020a). The updated results  
563 show that the significance of the global ST warming trend over the past century  
564 (1900–2017) remains the same as previous estimates, and that the recent warming  
565 trend since 1998 increases slightly and is statistically significant. Using the new  
566 dataset CMST, the trend of global mean STs over the period 1998-2012 was estimated  
567 to be a little higher than that of other existing datasets and more significant: It is 0.091  
568  $\pm 0.094^\circ\text{C}/\text{decade}$  when both the fitting and data uncertainties were considered, and  
569  $0.091 \pm 0.088^\circ\text{C}/\text{decade}$  when only the fitting uncertainty was considered as in the

570 AR5 IPCC report. This suggests that the recent temperature changes (including those  
571 record warm years at the end of the series) have likely brought the debate about the  
572 “warming hiatus” to an end. This is opposite to the previous understanding as  
573 described in IPCC AR5 and many other studies (but the AR5 does include a brief  
574 discussion on the uncertainty of trend in B.1 of the Summary for Policy Makers)  
575 (IPCC, 2013b).

576 Using these new datasets, we have presented an updated evaluation of global and  
577 hemispheric ST changes since 1900. When both the fitting and data uncertainties were  
578 considered, the warming trends of global mean STs for the periods 1900-2019,  
579 1951-2019, 1979-2019, and 1998-2019 are estimated to be  $0.091 \pm 0.011$ ,  $0.145 \pm$   
580  $0.019$ ,  $0.173 \pm 0.033$ , and  $0.194 \pm 0.083$  °C/decade, respectively. They are  
581  $0.091 \pm 0.008$ ,  $0.145 \pm 0.014$ ,  $0.173 \pm 0.026$  and  $0.195 \pm 0.063$  °C/decade when only the  
582 fitting uncertainty was considered.

583 The introduction of newly adjusted sea surface temperature (SST) data (Karl et  
584 al., 2015), with record-setting extreme global temperature for the recent six years  
585 (2014-2019), makes the formulation of the "warming hiatus" gradually fade away.

586 The newly released C-LSAT and CMST datasets support these results by increasing  
587 the warming trends during the period 1998-2012 (and of 1998-2017) than those in the  
588 previous versions of other existing observational datasets. However, more consistent  
589 trends have been found from the datasets when applying sampling bias correction  
590 using satellites, SAT observation in buoys, and reanalysis, which need to be more  
591 comprehensively validated in future with more new observations and improved  
592 reanalysis.

593

#### 594 **Acknowledgment**

595 This study is supported by the Natural Science Foundation of China (Grant: 41975105), the  
596 National Key R&D Program of China (Grant: 2018YFC1507705; 2017YFC1502301). And thanks  
597 Dr. Geert van Oldenborgh from Royal Netherlands Meteorological Institute (KNMI) for providing  
598 several global SAT/ST datasets on Climate Explorer website (<http://climexp.knmi.nl/>) for  
599 calculating the temperature change trends in this paper.

600

#### 601 **Reference**

602 Brohan P, Kennedy JJ, Harris I, Tett SFB, Jones PD. (2006) Uncertainty estimates in regional and global  
603 observed temperature changes: A new dataset from 1850. *J. Geophys. Res.* 111: D12106, doi:  
604 10.1029/2005JD006548.

605 Cahill N, S Rahmstorf and A Parnell, (2015) Change points of global temperature *Environ. Res. Lett.* 10  
606 084002, doi:10.1088/1748-9326/10/8/084002

607 Cowtan, K. & Way R. G. (2014) Coverage bias in the HadCRUT4 temperature series and its impact on  
608 recent temperature trends, *Quarterly Journal of Royal Meteorological Society*, 140, 1935–1944.  
609 doi:10.1002/qj.2297

610 Cowtan K, P Jacobs, P Thorne et al, (2018) Statistical analysis of coverage error in simple global  
611 temperature estimators, *Dynamics and Statistics of the Climate System*, 1–18  
612 doi:10.1093/climsys/dzy003

613 Dee D. P., Uppala S. M., Simmons A. J., Berrisford P., Poli P., Kobayashi S., Andrae U., Balmaseda M.  
614 A., Balsamo G., Bauer P., Bechtold P., Beljaars A. C. M., van de Berg L., Bidlot J., Bormann N.,  
615 Delsol C., Dragani R., Fuentes M., Geer A. J., Haimberger L., Healy S. B., Hersbach H., H'olm E.  
616 V., Isaksen L., K'allberg P., K"ohler M., Matricardi M., McNally A. P., Monge-Sanz B. M.,  
617 Morcrette J. J., Park B. K., Peubey C., de Rosnay P., Tavolato C., Th'epaut J. N., Vitart F. (2011)

618 The ERA-Interim reanalysis: Configuration and performance of the data assimilation system. Q. J.  
619 R. Meteorol. Soc. 137: 553–597, doi: 10.1002/qj.828.

620 Diggle P J, Liang K Y, Zeger S L. (1994) Analysis of Longitudinal Data. Oxford University Press.

621 Freeman, E., and Coauthors, (2017) ICOADS Release 3.0: A major update to the historical marine  
622 climate record. International J. Climatology, 37, 2211–2232, DOI: 10.1002/joc.4775.

623 Folland, C. K., and Coauthors, 2001: Observed climate variability and change. Climate Change 2001:  
624 The Scientific Basis, J. T. Houghton et al., Eds., Cambridge University Press, 99–181.

625 Fyfe JC, Meehl GA, England MH, Mann ME, Santer BD, Flato GM, Hawkins E, Gillett NP, Xie S-P,  
626 Kosaka Y, Swart NC. (2016) Making sense of the early-2000s warming slowdown. Nat. Clim.  
627 Change 6: 224–228, doi: 10.1038/nclimate2938.

628 Hansen J, Ruedy R, Glascoe J et al. (1999), GISS analysis of surface temperature change. J. Geophys.  
629 Res., 104: 30997-31022.

630 Hansen J, Ruedy R, Sato M et al. (2001), A closer look at United States and global surface temperature  
631 change. J. Geophys. Res., 106: 23947-23963.

632 Hansen, J., M. Sato, R. Ruedy, K. Lo, D. W. Lea, and M. Medina Elizade (2006), Global temperature  
633 change, Proc. Natl. Acad. Sci. U. S. A., 103, 14, 288–293, doi:10.1073/pnas.0606291103

634 Hansen J, R Ruedy, M Sato, K Lo (2010), Global surface temperature change, *Reviews Of*  
635 *Geophysics*, 48 (4), RG404:1-29, DOI: 10.1029/2010RG000345

636 Hartmann, D. L. In: *Climate Change (2013) The Physical Science Basis*. (eds Stocker, T. F. et al.), Ch. 2  
637 (Cambridge University Press, Cambridge, 2013).

638 Hawkins E D and Jones P D, (2013) Notes and Correspondence On increasing global temperatures: 75  
639 years after Callendar, *Q. J. R. Meteorol. Soc.* 139: 1961–1963

640 Hersbach, H., Bell, B., Berrisford, P., Hirahara, S., Horányi, A., Muñoz-Sabater, J., et al. (2020). The  
641 ERA5 Global Reanalysis. *Quarterly Journal of the Royal Meteorological*  
642 *Society*. doi:10.1002/qj.3803

643 Hirahara, S., M. Ishii, and Y. Fukuda, (2014) Centennial-scale sea surface temperature analysis and its  
644 uncertainty. *J. Climate*, 27, 57–75, doi:10.1175/JCLI-D-12-00837.1.

645 Huang B, MJ Menne, T Boyer, E Freeman, et al, (2019) Uncertainty estimates for sea surface  
646 temperature and land surface air temperature in NOAA GlobalTemp version 5, *J. Climate*, doi :  
647 10.1175/CLI-D-19-0395.1, in press.

648 Huang, B., P. W. Thorne, T. M. Smith, W. Liu, J. Lawrimore, V. F. Banzon, H.-M. Zhang, T. C. Peterson,  
649 and M. Menne, (2016) Further exploring and quantifying uncertainties for Extended Reconstructed



650 Sea Surface Temperature (ERSST) version 4 (v4). *J. Climate*, 29, 3119-3142, DOI:  
651 10.1175/JCLI-D-15-0430.1.

652 Huang, B., W. Angel, T. Boyer, L. Cheng, G. Chepurin, E. Freeman, C. Liu, and H.-M. Zhang, (2018)  
653 Evaluating SST analyses with independent ocean profile observations. *J. Climate*, 31, 5015-5030,  
654 doi:10.1175/jcli-d-17-0824.1.

655 Huang, B., P. Thorne, V. Banzon, T. Boyer, G. Chepurin, J. Lawrimore, M. Menne, T. Smith, R. Vose,  
656 and H. Zhang, (2017a) Extended Reconstructed Sea Surface Temperature version 5 (ERSSTv5):  
657 Upgrades, Validations, and Intercomparisons. *J. Climate*. 30, 8179-8205,  
658 doi:10.1175/JCLI-D-16-0836.1.

659 Huang, J., Zhang, X., Zhang, Q., et al. (2017b) Recently Amplified Arctic Warming Has Contributed  
660 to a Continual Global Warming Trend , *Nature Climate Change*, 7, 875–879.  
661 doi:10.1038/s41558-017-0009-5.

662 IPCC. 2007. *Climate Change (2007) The Physical Science Basis*. Contribution of Working Group I to the  
663 Fourth Assessment Report of the Intergovernmental Panel on Climate Change, Solomon S, Qin D,  
664 Manning M, Chen Z, Marquis M, Averyt KB, Tignor M, Miller HL. (eds.): 996 pp. Cambridge  
665 University Press: Cambridge, UK and New York, NY.

666 IPCC. 2013a. Climate Change (2013) The Physical Science Basis. Contribution of Working Group I to  
667 the Fifth Assessment Report of the Intergovernmental Panel on Climate Change, Stocker TF, Qin D,  
668 Plattner G-K, Tignor M, Allen SK, Boschung J, Nauels A, Xia Y, Bex V, Midgley PM. (eds.): 1535  
669 pp. Cambridge University Press: Cambridge, UK and New York, NY.

670 IPCC, 2013b. Summary for Policymakers. In: Climate Change (2013) The Physical Science Basis.  
671 Contribution of Working Group I to the Fifth Assessment Report of the Intergovernmental Panel on  
672 Climate Change [Stocker, T.F., D. Qin, G.-K. Plattner, M. Tignor, S.K. Allen, J. Boschung, A.  
673 Nauels, Y. Xia, V. Bex and P.M. Midgley (eds.)]. Cambridge University Press, Cambridge, United  
674 Kingdom and New York, NY, USA

675 Ishii, M., A. Shouji, S. Sugimoto, and T. Matsumoto, (2005) Objective analyses of sea-surface  
676 temperature and marine meteorological variables for the 20th century using ICOADS and the Kobe  
677 Collection. *Int. J. Climatol.*, 25, 865–879, doi:10.1002/joc.1169.

678 Jones P. D., L. David, T. J. Osborn, C. Harpham, M. Salmon, and C. P. Morice (2012), Hemispheric and  
679 large-scale land-surface air temperature variations: An extensive revision and an update to 2010. *J*  
680 *Geophys Res-Atmos*, 117, doi:10.1029/2011JD017139.

681 Jones, P. D., and T. M. L. Wigley (2010), Estimation of global temperature trends: What’s important and

682 what isn't, *Clim. Change*, 100(1), 59–69.

683 Jones P. D., Moberg A. (2003) Hemispheric and large-scale surface air temperature variations: an  
684 extensive revision and an update to 2001, *J Climate*, 16:206–223

685 Karl T.R., Arguez A., Huang B., Lawrimore J.H., McMahon J.R., Menne M.J., Peterson T.C., Vose R.S.,  
686 Zhang H.M. (2015) Possible artifacts of data biases in the recent global surface warming hiatus.  
687 *Science*, 348: 1469–1472. doi:10.1126/science.aaa5632

688 Kennedy, J. J., N. A. Rayner, R. O. Smith, D. E. Parker, and M. Saunby, (2011a) Reassessing biases and  
689 other uncertainties in sea surface temperature observations measured in situ since 1850: 2. Biases  
690 and homogenization. *Journal of Geophysical Research-Atmospheres*, 116, D14104,  
691 doi:10.1029/2010JD015220

692 Kennedy, J. J., N. A. Rayner, R. O. Smith, M. Saunby, and D. E. Parker (2011b) Reassessing biases and  
693 other uncertainties in sea surface temperature observations since 1850, part 1: Measurement and  
694 sampling uncertainties. *J. Geophys. Res.*, 116, D14103, doi:10.1029/2010JD015218

695 Kennedy, J. J. (2014) A review of uncertainty in in situ measurements and data sets of sea surface  
696 temperature, *Rev. Geophys.*, 52, 1–32, doi:10.1002/2013RG000434.

697 Kennedy, J. J., Rayner, N. A., Atkinson, C. P., & Killick, R. E. ( 2019) An ensemble data set of sea-

698 surface temperature change from 1850: the Met Office Hadley Centre HadSST.4.0.0.0 data set.  
699 Journal of Geophysical Research: Atmospheres, 124. <https://doi.org/10.1029/2018JD029867>

700 Kent, E. C., Kennedy, J. J., Smith, T. M., Hirahara, S., Huang, B., Kaplan, A., Parker, D. E., Atkinson, C.  
701 P., Berry, D. I., Carella, G., Fukuda, Y., Ishii, M., Jones, P. D., Lindgren, F., Merchant, C. J.,  
702 Morak-Bozzo, S., Rayner, N. A., Venema, V., Yasui, S., Zhang, H-M. (2017) A call for new  
703 approaches to quantifying biases in observations of sea-surface temperature. *Bulletin of the*  
704 *American Meteorological Society*, **98**, 1601-1616, doi:10.1175/BAMS-D-15-00251.1

705 Lawrimore J. H., M. J. Menne, B. E. Gleason, C. N. Williams, D. B. Wuertz, R. S. Vose, and J. Rennie  
706 (2011) An overview of the Global Historical Climatology Network monthly mean temperature data  
707 set, version 3. Journal of Geophysical Research-Atmospheres, 116, doi:10.1029/2011jd016187.

708 Lenssen, N., G. Schmidt, J. Hansen, M. Menne, A. Persin, R. Ruedy, and D. Zyss, (2019) Improvements  
709 in the GISTEMP uncertainty model. Journal of Geophysical Research-Atmospheres, 124, 12,  
710 6307-6326, doi:10.1029/2018JD029522.

711 Lewandowsky S., K Cowtan., J. Risbey, et al. (2018) The ‘pause’ in global warming in historical context:  
712 (II). Comparing models to observations. *Environ. Res. Lett.*, 13, 123007,  
713 <https://doi.org/10.1088/1748-9326/aaf372>.

714 Lewandowsky S., J. Risbey, and N. Oreskes (2016) The “pause” in global warming: Turning a routine  
715 fluctuation into a problem for science. *Bull. Amer. Meteor. Soc.*, 97, 723–733,  
716 doi:10.1175/BAMS-D-14-00106.1.

717 Li Q. and Y. Yang, (2019) Comments on “Comparing the current and early 20th century warm periods in  
718 China” by Soon W., R. Connolly, M. Connolly et al., *Earth-Science Reviews*, 198, 102886,  
719 <https://doi.org/10.1016/j.earscirev.2019.102886>

720 Li Q., Zhang L., Xu W. et al. (2017) Comparisons of time series of annual mean surface air temperature  
721 for China since the 1900s: Observation, Model simulation and extended reanalysis. *Bull. Amer.*  
722 *Meteor. Soc.*, 98 (4):699-711, doi: 10.1175/BAMS-D-16-0092.1

723 Li Q., S. Yang, W. Xu, X. L. Wang, P. Jones, D. Parker, L. Zhou, Y. Feng, and Y. Gao (2015) China  
724 experiencing the recent warming hiatus, *Geophys. Res. Lett.*, 42, doi:10.1002/2014GL062773.

725 Li Q., W. Dong, W. Li, X. Gao, P. Jones, J. Kennedy and D. Parker (2010) Assessment of the  
726 uncertainties in temperature change in China during the last century. *Chin. Sci. Bull.*, 55,  
727 1974-1982, doi: 10.1007/s11434-010-3209-1.

728 Li Q, Sun W, Huang B, Dong W, Wang X, Zhai P and P. Jones. (2020a) Consistency of global warming  
729 trends strengthened since 1880s, *Science Bulletin*, accepted.

730 Li Q., W. Dong and P. Jones (2020b) Continental Scale Surface Air Temperature Variations: An  
731 Experience Derived from China Region Practice, *Earth-Science Reviews*, 200, 998,  
732 <https://doi.org/10.1016/j.earscirev.2019.102998>.

733 Lugina, K. M., P. Y. Groisman, K. Y. Vinnikov, V. V. Koknaeva, and N. A. Sperandkaya (2006), Monthly  
734 surface air temperature time series area-averaged over the 30-degree latitudinal belts of the globe,  
735 1881–2005, in *Trends: A Compendium of Data on Global Change* [online],  
736 doi:10.3334/CDIAC/cli.003, Carbon Dioxide Inf. Anal. Cent., Oak Ridge Natl. Lab., U.S. Dep. Of  
737 Energy, Oak Ridge, Tenn. (Available at <http://cdiac.ornl.gov/trends/temp/lugina/lugina.html>)

738 Medhaug I, Stolpe M, Fischer E et al.  
739 (2017) Reconciling controversies about the 'global warming hiatus', *Nature*, 545: 41-47.  
740 DOI:10.1038/nature22315.

741 Morice, C. P., J. J. Kennedy, N. A. Rayner, and P. D. Jones (2012) Quantifying uncertainties in global and  
742 regional temperature change using an ensemble of observational estimates: The HadCRUT4  
743 dataset, *J. Geophys. Res.*, 117, D08101, doi:10.1029/2011JD017187.

744 Menne J. M., C. N. Williams, B. E. Gleason, et al. (2018) The Global Historical Climatology Network  
745 Monthly Temperature Dataset, Version 4, *J Climate*, 31 (24): 9835–9854.

746 <https://doi.org/10.1175/JCLI-D-18-0094.1>

747 Muller, R. A., J. Curry, D. Groom, R. Jacobsen, S. Perlmuter, R. Rohde, A. Rosenfeld, C. Wickham, and

748 J. Wurtele (2013) Decadal variations in the global atmospheric land temperatures, *J. Geophys. Res.*

749 *Atmos.*, 118, doi:10.1002/jgrd.50458.

750 Peterson T.C., and R.S. Vose (1997) An overview of the Global Historical Climatology Network

751 temperature database. *Bulletin of the American Meteorological Society*, 78, 2837-2849.

752 Peterson T. C., Willett K. M., Thorne P. C. (2011) Observed changes in surface atmospheric energy over

753 land. *Geophys. Res. Lett.* 38: L16707, doi:10.1029/2011GL048442.

754 Rahmstorf S, G Foster and N Cahill (2017) Global temperature evolution: recent trends and some pitfalls.

755 *Environ. Res. Lett.*, 12 054001, <https://doi.org/10.1088/1748-9326/aa6825>

756 Rayner, N. A., P. Brohan, D. E. Parker, C. K. Folland, J. J. Kennedy, M. Vanicek, T. J. Ansell, and S. F. B.

757 Tett (2006) Improved analyses of changes and uncertainties in sea-surface temperature measured

758 in-situ since the mid-nineteenth century, *J. Clim.*, 19, 446 – 469.

759 Risbey J., S. Lewandowsky, K Cowtan., et al. (2018), A fluctuation in surface temperature in historical

760 context: reassessment and retrospective on the evidence. *Environ. Res. Lett.*, 13, 123008,

761 <https://doi.org/10.1088/1748-9326/aaf342>.

762 Rohde R., Muller, R. A., Jacobsen, R., et al. (2013), A new estimate of the average earth surface land  
763 temperature spanning 1753 to 2011. *Geoinfor Geostat: An Overview*. doi:10.4172/gigs.1000101.

764 Simmons, A.J., Berrisford, P., Dee, D.P., Hersbach, H., Hirahara, S. and Thépaut, J.N. (2017) A  
765 reassessment of temperature variations and trends from global reanalyses and monthly surface  
766 climatological datasets. *Quarterly Journal of the Royal Meteorological Society*, 143: 101-119,. doi:  
767 <https://doi.org/10.1002/qj.2949>

768 Simons AJ, Willett KM, Jones PD, Thorne PW, Dee DP. (2010). Low-frequency variations in surface  
769 atmospheric humidity, temperature and precipitation: Inferences from reanalyses and monthly  
770 gridded observational datasets. *J. Geophys. Res.* 115: D01110, doi: 10.1029/2009JD012442.

771 Stott, P.A. & Thorne, P.W. (2010) How best to log local temperatures? *Nature*, 465:158-159.

772 Smith, T., R. W. Reynolds, R. E. Livezey, and D. C. Stokes (1996) Reconstruction of historical sea  
773 surface temperatures using empirical orthogonal functions. *J. Climate*, 9, 1403–1420, doi:10.1175/  
774 1520-0442(1996)009,1403: ROHSST.2.0.CO;2.

775 Smith, T. M., and R. W. Reynolds (2005) A global merged land-air-sea surface temperature  
776 reconstruction based on historical observations (1880–1997), *J. Clim.*, 18, 2021–2036,  
777 doi:10.1175/JCLI3362.1.



778 Smith, T., R. W. Reynolds, T. C. Peterson, and J. Lawrimore (2008) Improvements to NOAA's historical  
779 merged land–ocean surface temperature analysis (1880–2006). *J. Climate*, 21, 2283–2296,  
780 doi:10.1175/2007JCLI2100.1

781 Titchner, H. A., and N. A. Rayner (2014) The Met Office Hadley Centre sea ice and sea surface  
782 temperature data set, version 2: 1. Sea ice concentrations, *J. Geophys. Res. Atmos.*, 119, 2864–2889,  
783 doi: 10.1002/2013JD020316.

784 Trenberth K. T., P. Stepaniak, and S. Worley (2002) Evolution of El Niño  
785 -Southern Oscillation and global atmospheric surface temperatures, *J. Geophys. Res.* 107, D8,  
786 4065, 10.1029/2000JD000298

787 Vose, R. S., et al. (2012) NOAA's Merged Land-Ocean Surface Temperature Analysis. *Bulletin of the*  
788 *American Meteorological Society*, doi:10.1175/BAMS-D-11-00241.1.

789 Xu W., Q. Li, P. D. Jones, X. L. Wang, et al. (2018) A new integrated and homogenized global monthly  
790 land surface air temperature dataset for the period since 1900, *Clim. Dynamics*, 50:2513–2536,  
791 10.1007/s00382-017-3755-1.

792 Yun, X., Huang, B., Cheng, J., Xu, W., Qiao, S., and Li, Q. (2019) A new merge of global surface  
793 temperature datasets since the start of the 20th Century, *Earth Syst. Sci. Data*, 11, 1629–1643,

- 794 <https://doi.org/10.5194/essd-11-1629-2019>
- 795 Zhai P., Yu. R., Guo Y., Li Q., Ren X., Wang Y., Xu W., Liu Y., Ding Y. (2016) The strong El Niño in
- 796 2015/2016 and its dominant impacts on global and China's climate. *J. Meteorol. Res.*, 74(3): 309–
- 797 321. doi:10.11676/qxxb2016.049
- 798 Zhang, H.-M., J. H. Lawrimore, B. Huang, M. J. Menne, X. Yin, A. SÃ¡nchez-Lugo, B. E. Gleason, R.
- 799 Vose, D. Arndt, J. J. Rennie, and C. N. Williams, (2019) Updated temperature data give a sharper
- 800 view of climate trends. *EOS*, 100, doi:10.1029/2019EO128229.
- 801

802 List of Tables

803

804 Table 1. Long-term trends and uncertainty of global land temperature over the indicated periods (°

805 C / 10a)

806 Table 2. Century-scale trends in global LSAT change from different datasets (°C / decade)

807 Table 3. Century-scale trends in annual global ST change from different datasets (°C / decade)

808 Table 4. Century-scale trends in global, Hemispheric and Tropical Belt ST change (°C / decade)

809 Table 5. GMST change trends (different uncertainties evaluation) with different SST datasets (°C /

810 decade)

811

812 Table1 Long-term trends and uncertainty of global land temperature over the indicated periods (°  
813 C / 10a)

<b>Period</b>	<b>Warming periods</b>			
	1850-2019	1901-2019	1951-2019	1979-2019
<b>Trend</b>	0.081±0.014	0.119±0.023	0.219±0.042	0.296±0.077

814  
815

816  
817

Table 2. Century-scale trends in global LSAT change from different datasets ( $^{\circ}\text{C} / \text{decade}$ )

	1900-2017	1951-2017	1979-2017	1998-2017	1998-2012
C-LSAT	0.100±0.012	0.188±0.024	0.274±0.040	0.247±0.098	0.120±0.120
CRUTEM4.6	0.101±0.012	0.192±0.024	0.279±0.042	0.236±0.110	0.106±0.138
GHCNv3	0.103±0.014	0.207±0.026	0.280±0.044	0.224±0.112	0.052±0.118
GISTEMPv3 (250)	—	0.195±0.026	0.272±0.046	0.241±0.108	0.090±0.122
GISTEMPv3 (1200)	0.098±0.010	0.185±0.020	0.227±0.036	0.203±0.098	0.093±0.120
Berkeley SAT	0.106±0.014	0.194±0.026	0.285±0.048	0.246±0.114	0.161±0.164

818  
819

820  
821

Table 3. Century-scale trends in annual global ST change from different datasets ( $^{\circ}\text{C} / \text{decade}$ )

	1900-2017	1951-2017	1979-2017	1998-2017	1998-2012
CMST	0.086±0.008	0.133±0.014	0.164±0.026	0.190±0.072	0.091±0.088
HadCRUT4	0.079±0.008	0.120±0.016	0.174±0.026	0.147±0.074	0.055±0.094
NOAAGlobalTemp	0.085±0.008	0.138±0.014	0.165±0.024	0.175±0.066	0.084±0.080
GISSv3 (250)	0.078±0.006	0.121±0.014	0.151±0.024	0.134±0.066	0.036±0.080
GISSv3 (1200)	0.086±0.008	0.136±0.014	0.177±0.026	0.154±0.072	0.071±0.094
BE1	0.082±0.006	0.116±0.016	0.188±0.028	0.183±0.074	0.110±0.102
BE2	0.090±0.008	0.130±0.016	0.166±0.026	0.163±0.070	0.079±0.094
ERA5	—	—	0.180±0.032	0.223±0.086	0.140±0.112
HadCRUT Hybrid	—	—	0.189±0.026	0.183±0.070	0.120±0.098

822  
823

824  
825

Table 4. Century-scale trends in global, Hemispheric and Tropical Belt ST change ( $^{\circ}\text{C} / \text{decade}$ )

	1900-2019	1951-2019	1979-2019	1998-2019	1998-2012
NH	$0.099 \pm 0.011$	$0.165 \pm 0.022$	$0.248 \pm 0.036$	$0.258 \pm 0.086$	$0.134 \pm 0.102$
SH	$0.077 \pm 0.006$	$0.113 \pm 0.011$	$0.079 \pm 0.020$	$0.125 \pm 0.055$	$0.041 \pm 0.098$
Tropical Belt	$0.081 \pm 0.009$	$0.130 \pm 0.018$	$0.147 \pm 0.034$	$0.186 \pm 0.098$	$0.072 \pm 0.165$

826  
827

828 Table 5. GMST change trends (different uncertainties evaluation) with different SST datasets (°C /  
 829 decade)  
 830

Uncertainties		1900-2019	1951-2019	1979-2019	1998-2019	1998-2012
Merge1 (CMST)	Fitting	0.091±0.008	0.145±0.014	0.173±0.026	0.195±0.063	0.091±0.088
	Fitting+data	0.091±0.011	0.145±0.019	0.173±0.033	0.194±0.083	0.091±0.094
Merge2	Fitting	0.089±0.010	0.141±0.019	0.209±0.031	0.182±0.074	0.069±0.106
	Fitting+data	0.089±0.012	0.140±0.025	0.208±0.035	0.182±0.094	0.069±0.115

831

832



833 **List of Figures**

834 Figure 1 The flowchart of the approach of calculating data uncertainty.

835 Figure 2 The GLSAT anomaly series and its 95% confidence uncertainty range (a: GLSAT with  
836 the error ranges); b: GLSAT series without the error ranges. The anomaly is relative to the  
837 1961-1990 period.

838 Figure 3 Distribution of the linear trends of SAT in all grid boxes for different datasets (a. C-LSAT;  
839 b. CRUTEM4.6; c. GHCNv3; d. GISTEMPv3 (250km); e. GISTEMPv3 (1200km); f.  
840 Berkeley SAT. Unit: 0.1 °C/decade)

841 Figure 4 Annual mean LSAT anomalies (°C) and the linear trends during 1998–2012 (2017) in  
842 Arctic (a) and in Globe (b) (relative to 1961-1990)

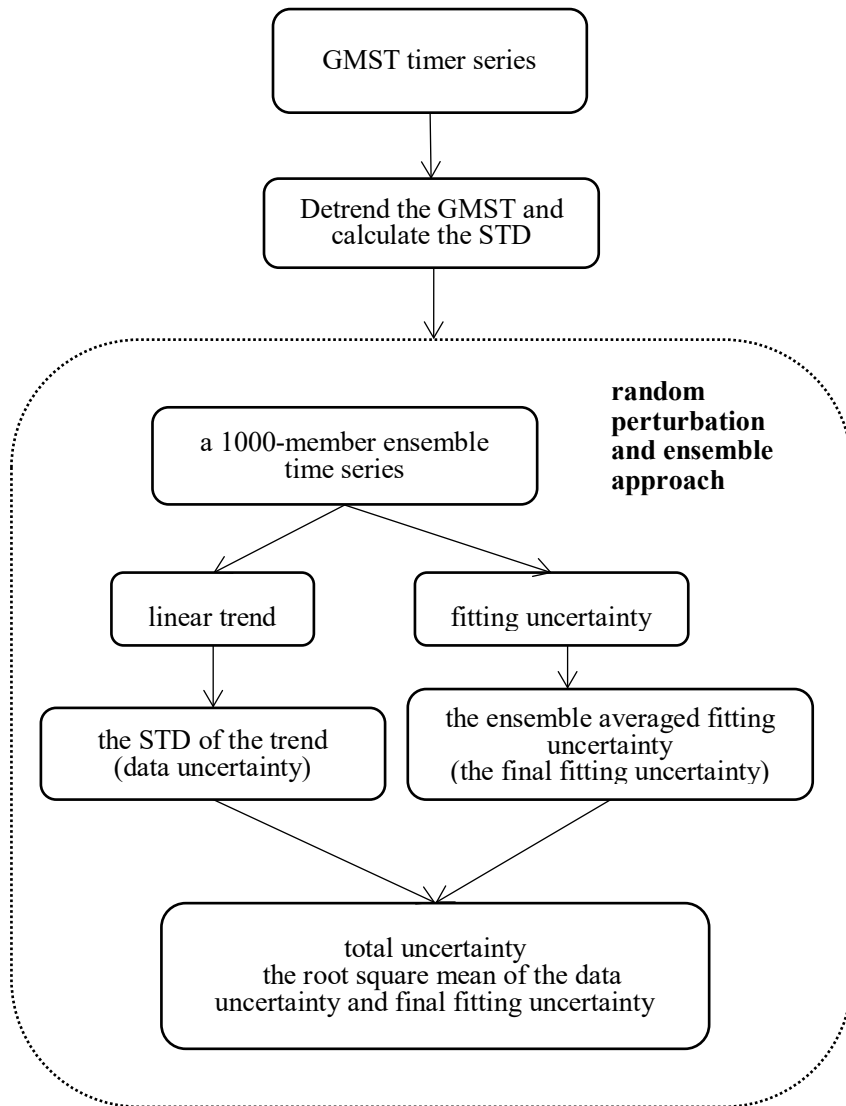
843 Figure 5 The distribution of the linear trends of ST in all grid boxes during 1998-2012 for different  
844 datasets (a. CMST; b. HadCRUT4; c. NOAAGlobalTemp; d. BE1; e. BE2; f. GISSv3 (1200);  
845 g. GISSv3 (250); h. HadCRUT Hybrid; i. ERA5. Unit: 0.1 °C/decade)

846 Figure 6 Global mean ST anomalies (°C) during 1998–2012 for 8 different datasets (the anomalies  
847 of ERA5/HadCRUT Hybrid (dashed lines) are relative to 1979-1990, the rest are relative to  
848 1961-1990)

849 Figure 7 Comparisons of the global mean ST change series between CMST and other 5 existing  
850 datasets.

851 Figure 8 Gobal (a), North Hemispheric (b), South Hemispheric (c) and Tropics (d) annual mean  
852 ST anomalies (°C) during 1900-2017 in CMST (the dashed line are linear trends)

853 Figure 9 Comparisons of global mean ST change merged with ERSSTv5 and median of HadSST3  
854 (a. ST change series; b. the differences)



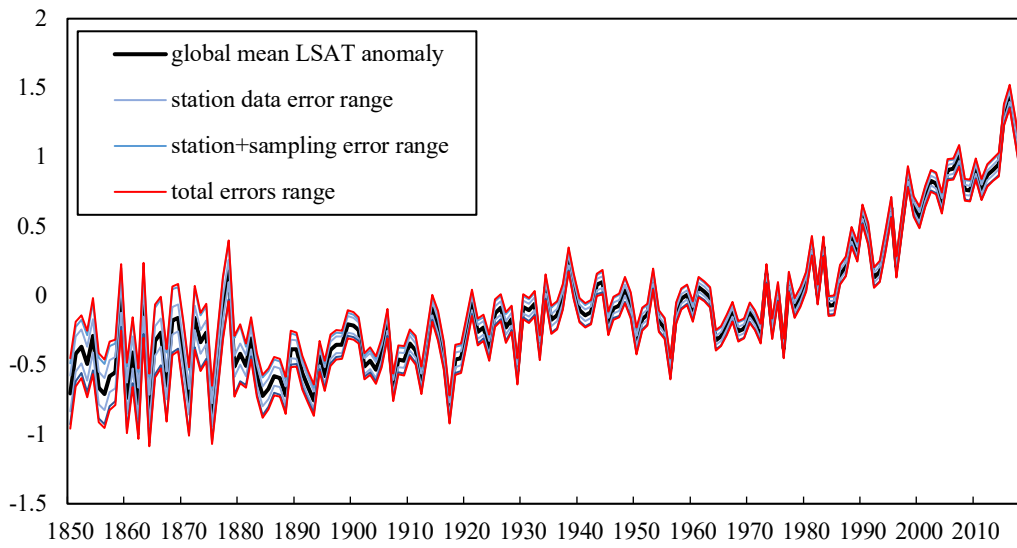
855

856

857

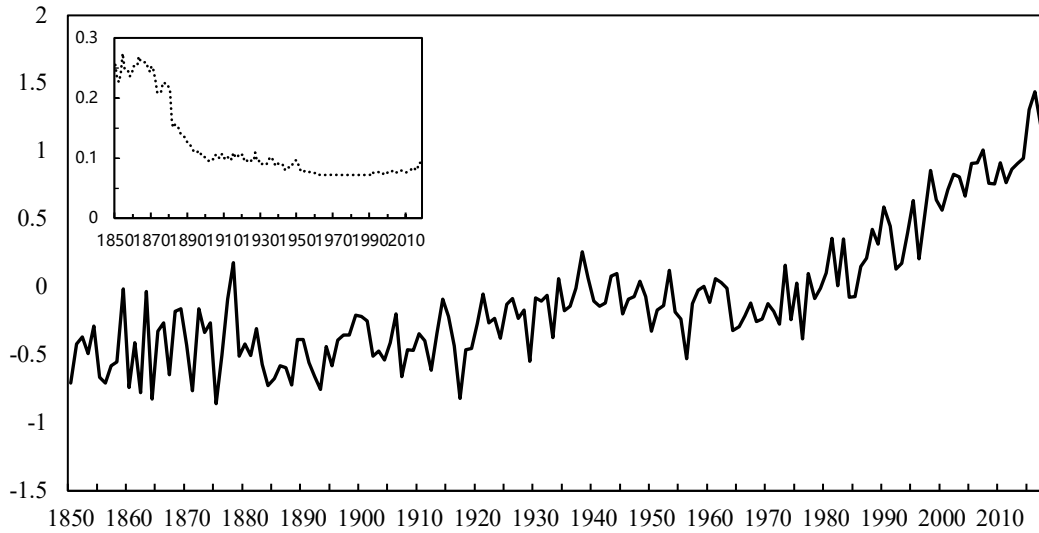
Figure 2 The flowchart of the approach of calculating data uncertainty.

**(a) Global Land Surface Air Temperature change and uncertainties**



858

**(b) Global Land Surface Air Temperature change**



859

860

861

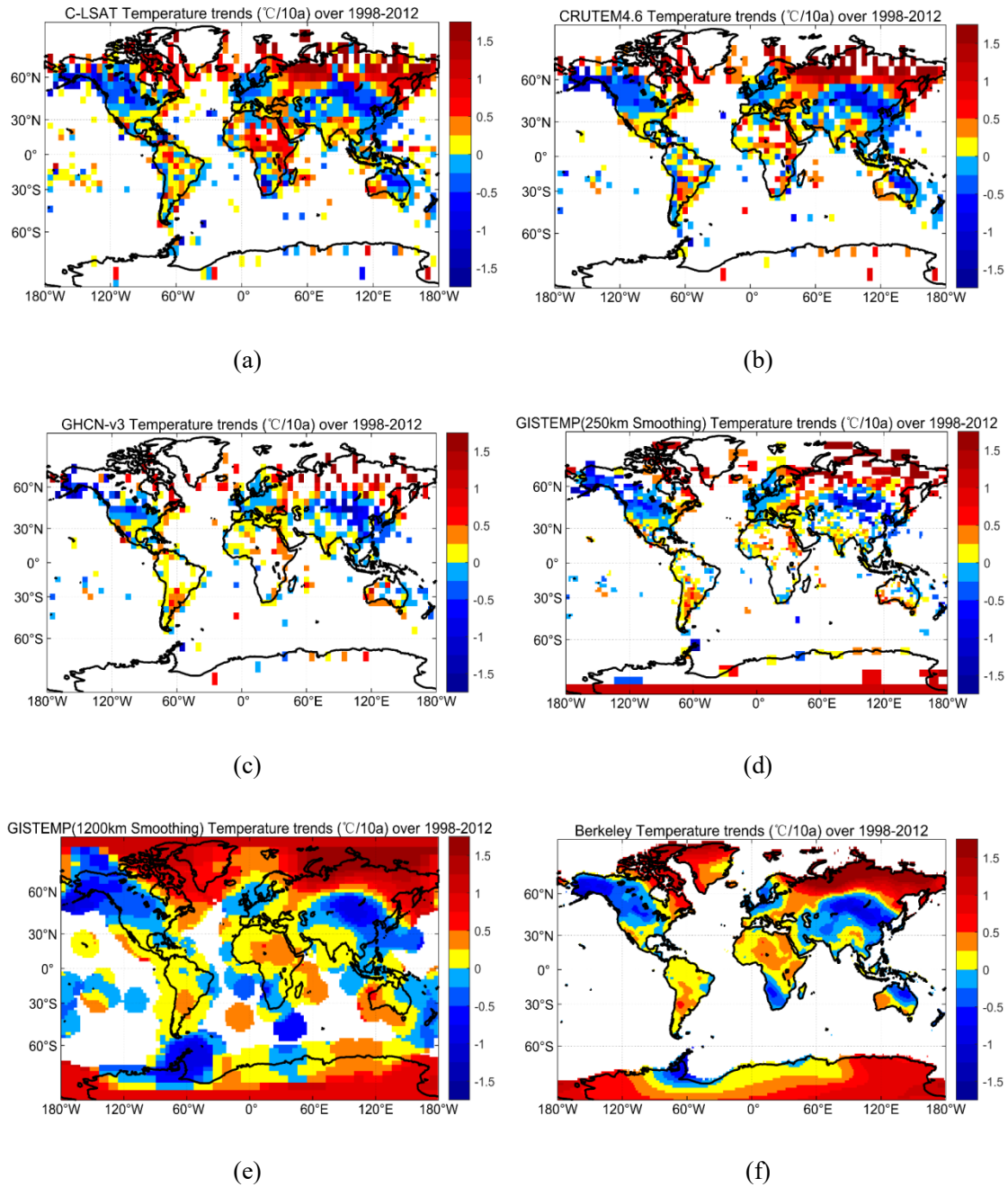
862

863

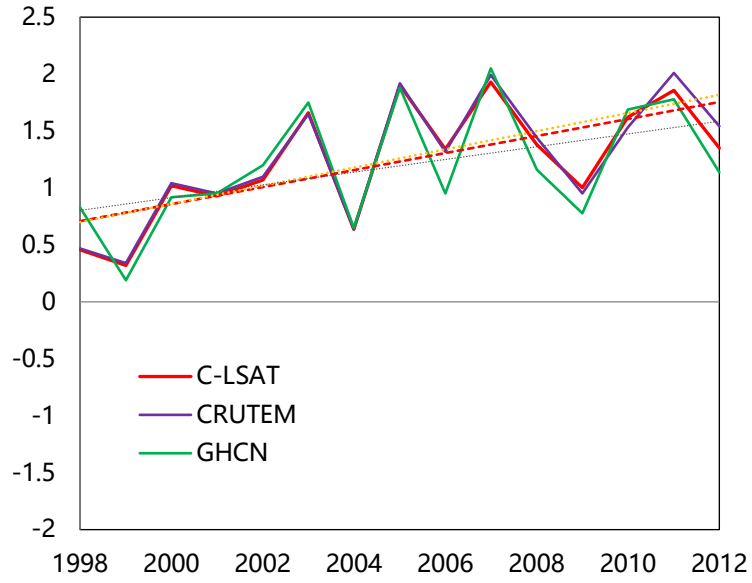
864

865

Figure 2 The GLSAT anomaly series and its 95% confidence uncertainty range (a: GLSAT with the error ranges); b: GLSAT series without the error ranges. The anomaly is relative to the 1961-1990 period. The inset in the upper panel shows the uncertainty ranges from different types of errors; and the inset in the lower panel shows the time series of the total error range.

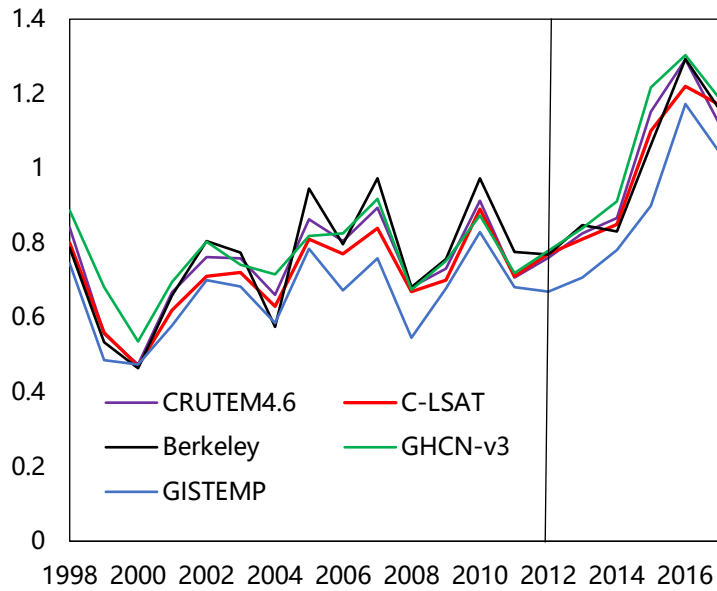


866 Figure 3 Distribution of the linear trends of SAT in all grid boxes for different datasets (a. C-LSAT;  
 867 b. CRUTEM4.6; c. GHCNv3; d. GISTEMPv3 (250km); e. GISTEMPv3 (1200km); f.  
 868 Berkeley SAT. Unit: 0.1 °C/decade)  
 869



870  
871

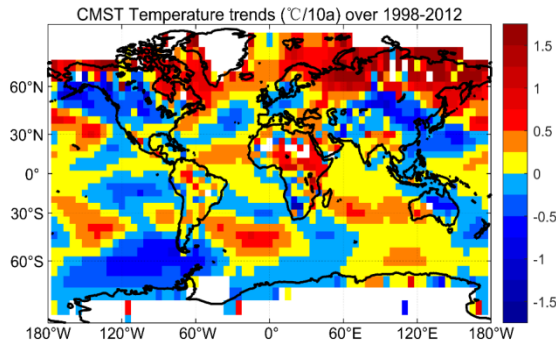
(a)



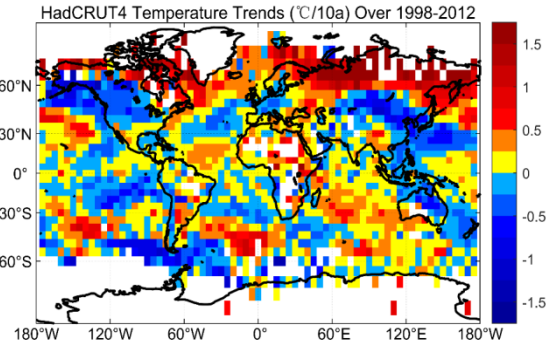
872  
873  
874  
875  
876

(b)

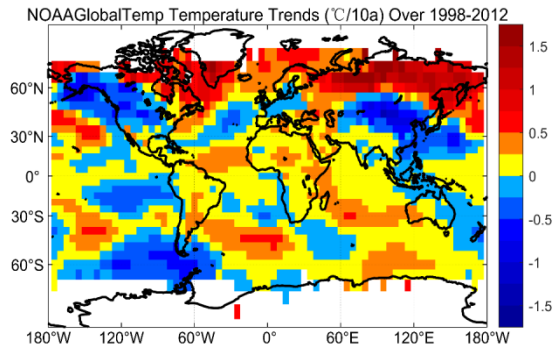
Figure 4 Annual mean LSAT anomalies ( $^{\circ}\text{C}$ ) during 1998–2012 in Arctic (a) and during 1998–2017 in Globe (b) (relative to 1961–1990)



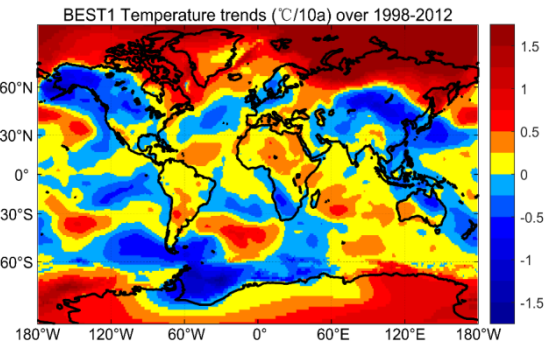
(a)



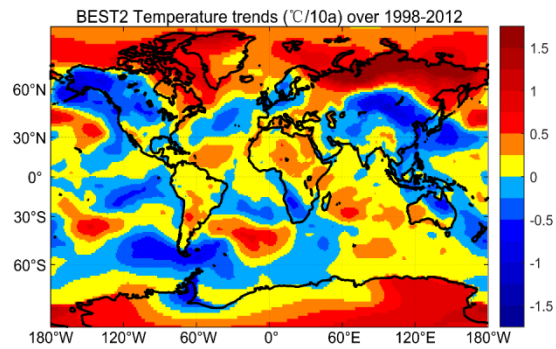
(b)



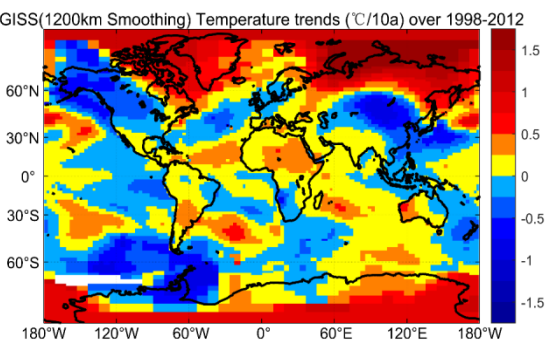
(c)



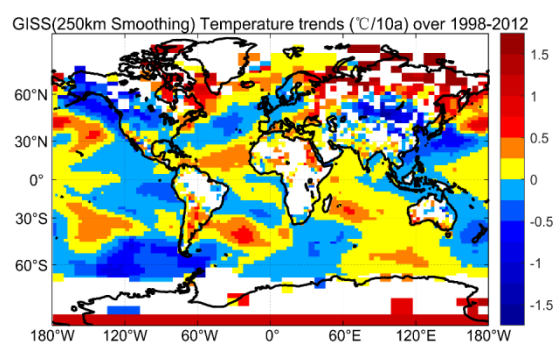
(d)



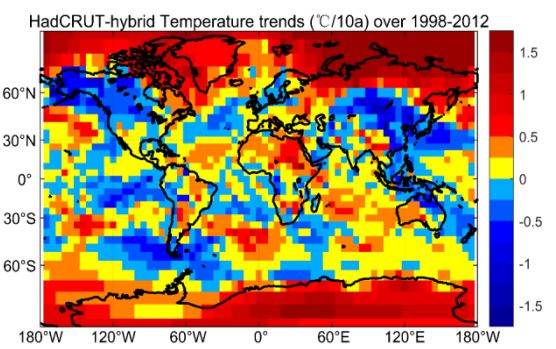
(e)



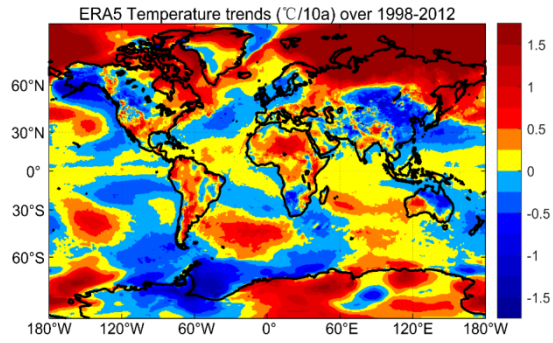
(f)



(g)



(h)



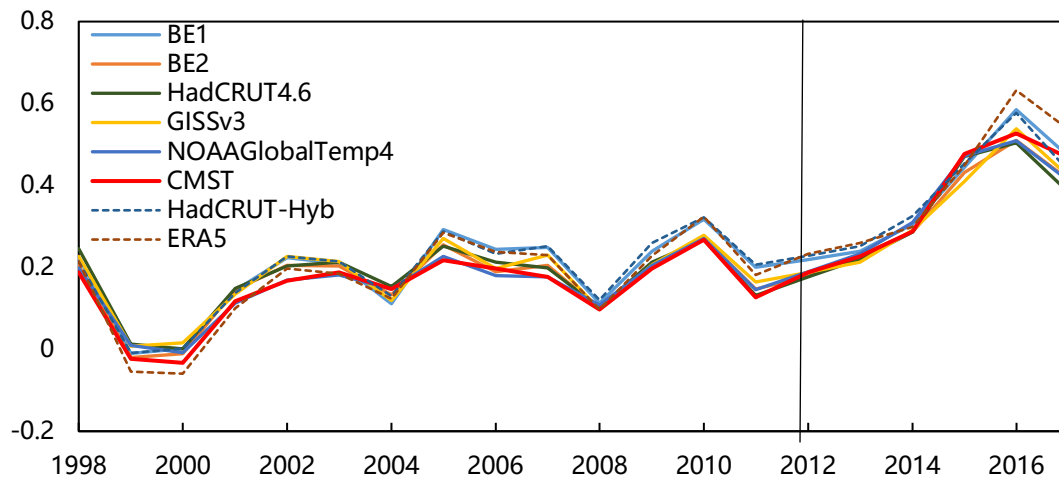
(i)

877 Figure 5 The distribution of the linear trends of ST in all grid boxes during 1998-2012 for different  
 878 datasets (a. CMST; b. HadCRUTEM4; c. NOAAGlobalTemp; d. BE1; e. BE2; f. GISS (1200); g.  
 879 GISS (250); h. HadCRUT Hybrid; i. ERA5. Unit: 0.1 °C/decade)

880

881

882



883

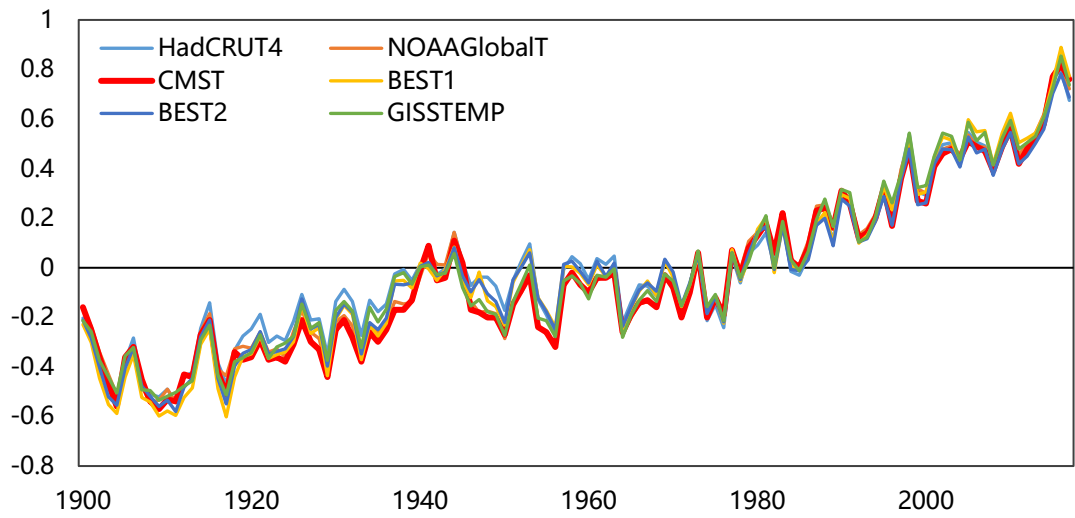
884

Figure 6 Global annual mean ST anomalies (°C) during 1998–2012 for 8 different datasets (the anomalies are all relative to 1981-2010)

885

886





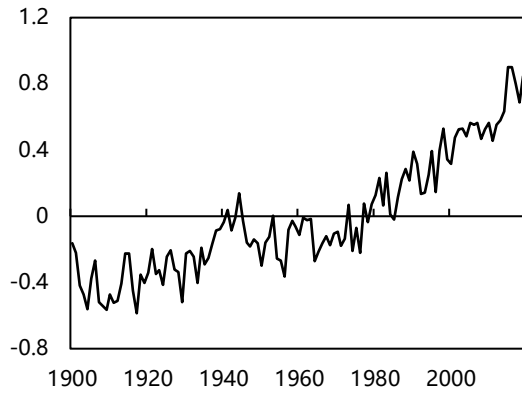
887

888

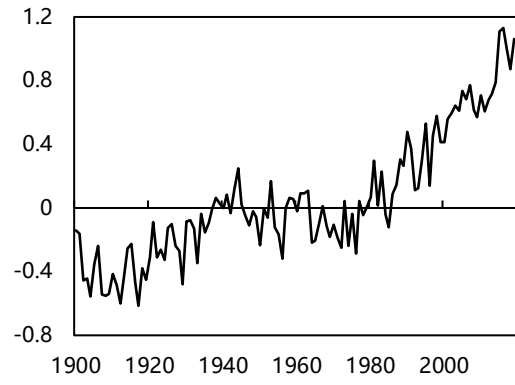
889 Figure 7 Comparisons of the global mean ST change series between CMST and other 5 existing

890 datasets.

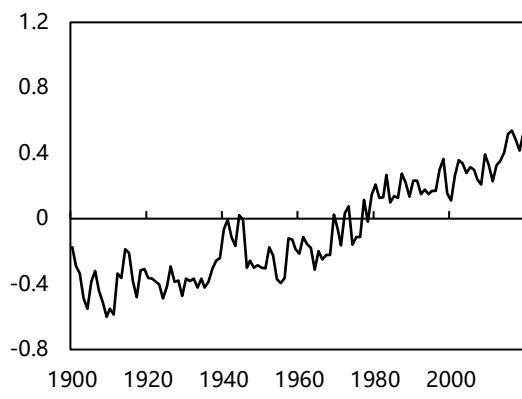
891



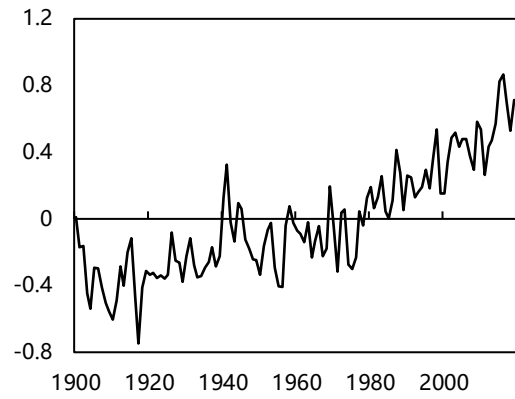
(a)



(b)

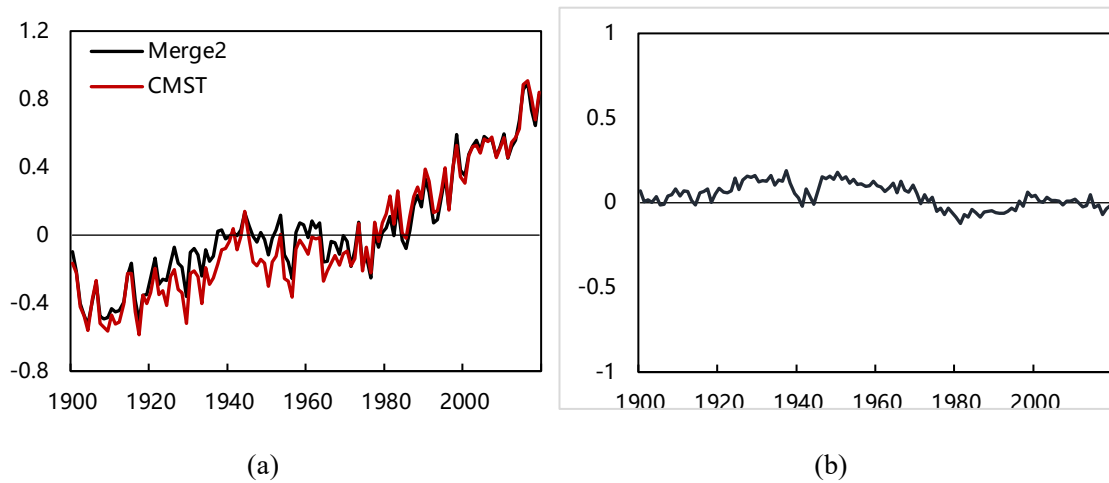


(c)



(d)

892 Figure 8 Global (a), North Hemispheric (b), South Hemispheric (c) and Tropical Belt (d) annual  
 893 mean ST anomalies ( $^{\circ}\text{C}$ ) during 1900-2017 in CMST (the dashed lines are linear trends)  
 894



895 Figure 9 Comparisons of global mean ST change merged with ERSSTv5 and median of HadSST3  
 896 (a. ST change series; b. the differences)  
 897